## References


1. Lazarus SS, Trombetta LD. Ultrastructural identification of a benign perineurial cell tumor. Cancer 1978;41:1823–9
2. Fetsch JF, Miettinen M. Sclerosing perineurioma: a clinicopathologic study of 19 cases of a distinctive soft tissue lesion with a predilection for the fingers and palms of young adults. Am J Surg Pathol 1997;21:1433–42
3. Yamaguchi U, Hasegawa T, Hirose T, et al. Sclerosing perineurioma: a clinicopathological study of five cases and diagnostic utility of immunohistochemical staining for GLUT1. Virchows Arch 2003;443:159–63
4. Canales-Ibarra C, Magarinos G, Olsoff-Pagovich P, Ortiz-Hidalgo C. Cutaneous sclerosing perineurioma of the digits: an uncommon soft-tissue neoplasm. Report of two cases with immunohistochemical analysis. J Cutan Pathol 2003;30:577–81
5. Huang HY, Sung MT. Sclerosing perineuriomas affecting bilateral hands. Br J Dermatol 2002;146:129–33
6. Hirose T, Tani T, Shimada T, Ishizawa K, Shimada S, Sano T. Immunohistochemical demonstration of EMA/GLUT1-positive perineurial cells and CD34 positive fibroblastic cells in peripheral nerve sheath tumors. Mod Pathol 2003;116:293–8
7. Sundaram M, McGuire MH, Schajowicz F. Soft tissue masses: histologic basis for decreased signal (short T2) on T2-weighted MR images. AJR 1987;148:1247–50
8. Karasick D, Karasick S. Giant cell tumor of tendon sheath: spectrum of radiologic findings. Skelet Radiol 1992;21:219–24
9. Horcajadas AB, Lafuente JL, de la Cruz Burgos R, et al. Ultrasound and MR findings in tumor and tumor-like lesions of the fingers. Eur Radiol 2003;13:672–85
10. Kato K, Ehara S, Nishida J, et al. Rapid involution of proliferative fasciitis. Skelet Radiol 2004;33:300–2

# Disease activity and $^{18}$F-FDG uptake in organising pneumonia: semi-quantitative evaluation using computed tomography and positron emission tomography

Ukihide Tateishi[1], Tadashi Hasegawa[2], Kunihiko Seki[3], Takashi Terauchi[4], Noriyuki Moriyama[4], Yasuaki Arai[1]

[1] Division of Diagnostic Radiology, National Cancer Center Hospital, Tsukiji, Chuo-ku, 104-0045 Tokyo, Japan
[2] Department of Clinical Pathology, Sapporo Medical University School of Medicine, Sapporo, Japan
[3] Pathology Division, National Cancer Center Hospital, Tokyo, Japan
[4] Division of Radiology, Research Center for Cancer Prevention and Screening, National Cancer Center, Tokyo, Japan

Received: 29 August 2005 / Accepted: 5 January 2006 / Published online: 28 March 2006


**Abstract.** *Purpose:* The present study was conducted to evaluate whether $^{18}$F-fluorodeoxyglucose positron emission tomography (FDG-PET) in combination with computed tomography (CT) reflects disease activity in patients with organising pneumonia.
*Methods:* Eighty-eight subjects who were normal ($n$=66) or who had proven organising pneumonia ($n$=22) underwent FDG-PET and CT imaging. The subjects included 55 men and 33 women, ranging in age from 24 to 63 years (mean 47 years). PET and CT data sets were digitally fused using a conformational PET/CT fusion algorithm. All scans were evaluated independently by two chest radiologists who were unaware of other clinical data. The visual score, maximal and mean standardised uptake value (SUV), and maximal and mean lesion-to-normal tissue ratio (LNR) were calculated. The imaging results were compared with the laboratory and pulmonary function test results. The inflammatory cells in the lesions were quantified immunohistochemically.
*Results:* The visual score, maximal and mean SUV, and maximal and mean LNR of the patients with organising pneumonia were significantly higher than those of the normal subjects. The patients with air-space consolidation had a significantly higher SUV than those without air-space consolidation (mean±SD 3.08±0.39 vs 2.35±0.56; $p$<0.05). The number of CD45$^+$ cells was positively correlated with the maximal SUV ($r$=0.632, $p$<0.01) and the maximal LNR ($r$=0.453, $p$<0.05). The number of CD8$^+$ T lymphocytes also showed positive correlations with the maximal SUV ($r$=0.540, $p$<0.01) and the maximal LNR ($r$=0.547, $p$<0.01).
*Conclusion:* Patients with organising pneumonia have an enhanced FDG accumulation which reflects the degree of disease activity.

*Keywords:* $^{18}$F-FDG PET – CT – Chest medicine – Organising pneumonia – Disease activity

**Eur J Nucl Med Mol Imaging (2006) 33:906–912**
DOI 10.1007/s00259-006-0073-y

Ukihide Tateishi (✉)
Division of Diagnostic Radiology,
National Cancer Center Hospital,
Tsukiji, Chuo-ku,
104-0045 Tokyo, Japan
e-mail: utateish@ncc.go.jp
Tel.: +81-3-35422511, Fax: +81-3-35423815

## Introduction

Organising pneumonia is characterised by the presence of buds of granulation tissue in the small airways comprising various degrees of interstitial and alveolar infiltration with mononuclear cells and alveolar macrophages [1–3]. Disease activity is correlated with the histological findings of organising pneumonia, which often reflect the incomplete resolution of inflammation leading to the development of fibrosis. Although the clinical course of organising pneumonia varies, the distinctive features of the sporadic onset of a flu-like illness accompanied by respiratory symptoms are often encountered. Organising pneumonia can also be a major histological reaction in various inflammatory processes, including connective tissue disease, drug reactions and infection [4–8].

Computed tomography (CT) findings in patients with organising pneumonia have been thoroughly described [9–15]. The most frequently observed appearance is a patchy area of air-space consolidation that tends to progress and change location over time [9–11]. A better characterisation of CT findings may help to manage patients with organising pneumonia, and the establishment of a reliable indicator will improve the monitoring of disease activity. However, focal lesions often appear as an ovoid mass in contact with the pleura and resembling lung cancer.

$^{18}$F-fluorodeoxyglucose (FDG) positron emission tomography (PET) can be effectively employed in patients with thoracic malignancies for diagnosis, staging, monitoring after treatment and the detection of recurrence. Nevertheless, multiple inflammatory processes can induce increased $^{18}$F-FDG uptake and create false positive results for thoracic malignancies. Various degrees of $^{18}$F-FDG uptake have been reported in infiltrative lung diseases, including idiopathic pulmonary fibrosis, collagen vascular disease-associated interstitial pneumonia, drug-induced pneumonia and radiation pneumonia [16–21]. However, organising pneumonia is not a well-known cause of increased $^{18}$F-FDG uptake and the relationship of the increased $^{18}$F-FDG uptake to clinical parameters and the pathological background has not been clearly identified.

The pioneering study by Majeski and co-workers examined and quantified the activity and progression of organising pneumonia in neonatally thymectomised CBA/J mice infected with reovirus 1/L [22]. The authors demonstrated that activated T lymphocytes provided a measure of disease activity in situ and concluded that the presence of T lymphocytes in the lung tissues of patients with organising pneumonia might indicate an important role in the modulation of disease progression. This previous report focussed on cellular infiltrates early during the inflammatory response in vitro but did not investigate the chronic behaviour of inflammatory cell subtypes, which are often found in pathological specimens obtained from patients with organising pneumonia.

The aim of the present study was to characterise and quantify disease activity in patients with organising pneumonia using co-registered $^{18}$F-FDG PET and CT images and comparing these imaging findings with those obtained in normal controls. We also examined the inflammatory cell infiltrates present in pathological specimens, since the histological subtypes of the inflammatory cells could play a role in the progression of the disease and could be correlated with the co-registered PET and CT findings.

## Materials and methods

Twenty-two subjects with organising pneumonia were recruited from our institution and were matched for age with a group of 66 normal subjects. $^{18}$F-FDG PET and CT were performed in all subjects in a systematic search for cancer, reflecting current practice in our country. A review of the pathological records confirmed that a diagnosis of organising pneumonia had been established in each patient by either a trans-bronchial lung biopsy ($n$=18) or an open lung biopsy ($n$=4). Among the subjects with organising pneumonia, ten exhibited cryptogenic organising pneumonia, nine exhibited organising pneumonia associated with collagen-vascular disease and three exhibited drug-induced organising pneumonia. The causative drugs were non-steroidal anti-inflammatory drugs, as determined by history of drug exposure in addition to a lymphocyte stimulation test with the drug in question. Subjects with a history of malignancy, diabetes, respiratory failure, heart failure or liver disease were not eligible for enrolment in this study.

None of the subjects with organising pneumonia had received any therapy prior to the present study. Pulmonary function tests, including measurements of forced vital capacity (FVC), $FEV_1$, functional residual capacity (FRC), residual volume (RV), total lung capacity (TLC) and carbon monoxide diffusing capacity ($D_{LCO}$), were performed using a computerised spirometer. The results were expressed in relation to the predicted values for age and height. Venous blood was obtained for routine blood tests, including the determination of C-reactive protein (CRP) levels and white blood cell counts (WBC). The serum concentration of KL-6, a circulating glycoprotein that is a sensitive marker of organising pneumonia (normal value less than 520 U/ml), was also determined. The present study conformed with the Declaration of Helsinki, and informed written consent was obtained from each subject. This study was approved by the local ethics committees after confirming that the subjects had provided their informed consent to a review of their medical records and images.

CT scans were acquired using a stacked multislice acquisition protocol on a 16 detector row CT scanner (Toshiba Medical Systems, Tokyo, Japan). A series of 1.0- and 5-mm-thick images were obtained using the following scan parameters: 120 kVp, 200–250 mA/rotation, 30–40 cm of field of view (FOV) and a 512×512 matrix. The subjects were examined while in a supine position, and none received a contrast material. Thin-section CT images were obtained using 2.0-mm sections reconstructed at 2.0-mm intervals by means of a high spatial frequency algorithm and were retrospectively retargeted to each lung with a 20-cm FOV. All examinations were performed from the apex to the base of the lungs. Images were reconstructed using a standard and a high spatial frequency algorithm at a display window width of 2,000 Hounsfield units (HU) and a window centre of −600 HU. All images were obtained with the subject in deep inspiration.

PET scanning was performed using dedicated PET scanners (ECAT ACCEL; Siemens/CTIMI, Knoxville, TN, USA). The transverse FOV was 16.2 cm, and 47 image planes were produced. To correct for photon attenuation, a transmission scan was obtained prior to the emission scan with 68 rotating germanium rod sources. Prior to the PET study, the patients fasted for at least 6 h. All patients were tested to ensure a normal glucose level (range 4.9–6.7 mmol/l) before PET scanning. Emission scans from the base of the skull to the mid-thigh were obtained starting 60–72 min after the intravenous administration of 300–346 MBq of $^{18}$F-FDG. Images were reconstructed with attenuation-weighted ordered-subset expectation maximisation with two iterations and eight subsets using the emission scans and reprojected attenuation maps as inputs.

An initial review of the attenuation-corrected PET images was performed using transaxial, coronal and sagittal planes. PET-CT fused images were available and were reviewed directly on the screen of the workstation. The images were reviewed by two board-certified radiologists who were unaware of clinical or radiological information, using hard-copy images in combination with a multimodality computer platform (syngo; Siemens, Knoxville, TN, USA). The observers assessed the presence of air-space consolidation, ground-glass attenuation, bronchial dilatation, small nodular lesions, band-like opacity and perilobular opacity. Areas of air-space consolidation were considered present when the opacity obscured the underlying vessels. Ground-glass attenuation was defined as an area of hazy increased parenchymal attenuation without obscuration of the underlying vascular markings. Small nodular lesions were defined as well-defined nodules less than approximately 10 mm in diameter. Band-like opacity was defined as smooth or irregular lines longer than 20 mm, sometimes forming arcades [11, 12]. Perilobular opacity was defined as linear opacity bordering the lobule, notably the interlobular septa or pleura [13]. Following an initial independent evaluation, the two observers reviewed all cases in which they had discrepant interpretations and reached a final decision by consensus.

Visual scores ranged from 1 to 5 as follows: 1=no sign of abnormality, 2=probably without abnormality, 3=indecisive concerning abnormality, 4=probable abnormality and 5=definite abnormality. For quantitative interpretation, a region of interest (ROI) analysis was performed. The ROI data were used to calculate standardised uptake values (SUVs) on the PET images. The ROI to measure the SUV was drawn to include the whole lesion in subjects with organising pneumonia. In addition, the ROI was used to evaluate the portion of the corresponding lung segment with 4×4 pixels in the control subjects. SUV was determined, according to the standard formula, as the activity in the ROI given in Bq/ml/injected activity in Bq/weight (kg). Additional SUV data were also obtained for a non-diseased segment of the lung. The maximal and mean pixel value with the ROI and the lesion-to-normal lung ratio (LNR) were recorded.

Tissue blocks obtained at biopsy were fixed in 4% formaldehyde using vacuum inflation, embedded in paraffin and processed into 4-μm-thick serial sections. Histochemical analysis was performed on sections stained with haematoxylin-eosin and elastic van Gieson. The infiltration of total leucocytes ($CD45^+$ cells), macrophages ($CD68^+$ cells), $CD4^+$ T lymphocytes and $CD8^+$ T lymphocytes in the pathological specimens was quantified using immunohistochemical analysis. The sections were dewaxed, rehydrated and moistened with phosphate-buffered saline (pH 7.4). They were then pretreated in an autoclave at 121°C for 10 min in 10 mmol/l citrate buffer (pH 6.0) before incubation. Mouse monoclonal antibodies were used to identify leucocytes (CD45, M0701; Dako), macrophages (CD68, M0814; Dako), $CD4^+$ T lymphocytes (CD4, M0834; Dako) and $CD8^+$ T lymphocytes (CD8, M7103; Dako) using an automated immunostaining system (i6000; BioGenex, San Ramon, CA, USA). Ten representative fields from the immunostained sections were obtained per patient and were examined at a magnification of 400× for the quantitative evaluation. Images of these fields were digitised using a digital camera system (Coolpix Microsystem IV; Nikon, Tokyo, Japan) and analysed by image-processing software (Mac Scope; Mitani, Fukui, Japan). The results were expressed as the number of cells per square millimetre of tissue examined. To improve the validity and reproducibility of the findings, the average number of cells per square millimetre was used to assess the results of the immunohistochemical analysis. Histological diagnosis and quantitative evaluation of the immunostained sections were performed by a histopathologist.

Information regarding symptoms and treatment were retrieved from clinical records and official population registries in all patients. The patients with cryptogenic organising pneumonia and organising pneumonia associated with collagen-vascular disease were treated with doses of prednisone of 1.0 mg/kg daily for 1–2 months. Blood was obtained for routine blood tests, including the determination of CRP levels and WBC counts every week after treatment. Follow-up CT and $^{18}$F-FDG PET images were obtained 1 month ($n$=12) and 2 months ($n$=10) after withdrawal of the implicated drug or steroid therapy.

### *Statistical analysis*

Correlations between the clinical or pathological values and the SUV were summarised using Pearson correlation coefficients. Clinical variables, pulmonary function test results and PET measurements were compared between groups using two-sample $t$ tests. Variables that were not normally distributed were compared using a Wilcoxon $W$ test. A $p$ value of <0.05 was considered statistically significant.

## Results

The clinical characteristics and outcomes of all the patients with organising pneumonia and the normal subjects are summarised in Table 1. There were 55 men (63%) and 33 women (37%). The mean age at the time of diagnosis was 47±7 years, ranging from 24 to 63 years. Sixty-eight subjects (77%) were non-smokers. The proportion of non-smokers was similar among women (78%) and men (76%). The proportion of current smokers was smaller in the control group: only two subjects (3%) were active smokers. The $D_{LCO}$ (% predicted) was lower in the patients with organising pneumonia than in the normal subjects. No differences in VC (% predicted), $FEV_1$ (% predicted) or $FEV_1$/FVC (%) were seen between the two groups. The patients with organising pneumonia had significantly higher CRP and WBC values, compared with the control group, but their serum KL-6 level was normal. The two groups were similar with regard to age, gender, height, weight, smoking history and oxygen saturation under room air.

The mean visual score of the patients with organising pneumonia was significantly higher than that of the normal subjects ($p$<0.01). The 22 patients with organising pneumonia had a visual score of greater than 4, whereas the 56 normal subjects had a visual score of less than 2. The median values of maximal SUV, mean SUV, maximal LNR and mean LNR for the entire study population were 0.53 (range 0.40–3.90), 0.38 (0.22–1.12), 0.77 (0.33–7.64) and 0.53 (0.19–2.11), respectively (Table 2). Significant differences in the mean values for all variables were found between the two groups. Significant correlations between the maximal SUV or the maximal LNR and the CRP level

**Table 1.** Patient characteristics

| | Patients with organising pneumonia | Controls | $p$ Value |
|---|---|---|---|
| No. of subjects examined | 22 | 66 | |
| Age (years) | 47.3±2.0 | 46.3±0.8 | NS |
| No. of females/males | 10/12 | 23/43 | NS |
| Smoking history (pack-years) | 5.5±1.8 | 3.5±0.9 | NS |
| VC (% predicted) | 90.8±5.9 | 88.7±1.6 | NS |
| $FEV_1$ (% predicted) | 81.1±5.5 | 78.4±2.3 | NS |
| $FEV_1$/FVC (%) | 81.5±1.2 | 83.6±0.7 | NS |
| $D_{LCO}$ (% predicted) | 87.9±1.7 | 92.8±1.1 | <0.05 |
| Saturation (%) | 99.8±0.1 | 99.7±0.1 | NS |
| KL-6 (U/ml) | 298.6±17.6 | 268.0±15.0 | NS |
| CRP (mg/dl) | 2.4±0.2 | 0.0±0.0 | <0.0001 |
| WBC (/mm$^3$) | 7,271.3±220.5 | 4,733.2±41.9 | <0.0001 |

Values are expressed as mean ± standard deviation unless otherwise indicated

*VC* vital capacity, *$FEV_1$* forced expiratory volume per 1 s, *FVC* forced vital capacity, *$D_{LCO}$* carbon monoxide diffusing capacity, *CRP* C-reactive protein, *WBC* white blood cell count, *NS* not significant

were seen only in the patients with organising pneumonia. No significant relationships were seen between the PET measurements and the pulmonary function test results, oxygen saturation under room air, serum KL-6 level or WBC.

A good inter-observer agreement was obtained for the analysis of the CT findings (weighted kappa 0.63–0.78). Among the patients with organising pneumonia, common CT findings included air-space consolidation, ground-glass attenuation and bronchial dilatation (Table 3). Air-space consolidation was predominantly peripheral and was often associated with areas of ground-glass attenuation and bronchial dilatation (Fig. 1). Less common CT findings included band-like opacity, small nodular lesions and perilobular opacity. Band-like opacity was predominantly peripheral and located in the lower zone. The patients with air-space consolidation had a significantly higher maximal SUV than those without consolidation (mean±SD 3.08±0.39 vs 2.35±0.56; $p<0.05$). However, no other significant correlations were seen between the maximal SUV and CT findings.

Tissue specimens were characterised according to the presence of granulation comprising variable infiltrates of lymphocytes, macrophages and neutrophils (Fig. 1). The lesions were admixed with fibrin exudates and collagen-containing fibroblasts, embedded in a tissue matrix. Minor infiltration of the lesion by plasma cells and eosinophils was also found. The results of the cell counts in the lesions are shown in Table 4. Increased numbers of leucocytes ($CD45^+$ cells), macrophages ($CD68^+$ cells), CD4 T lymphocytes and CD8 T lymphocytes were observed (Fig. 1). The number of $CD45^+$ cells infiltrating the lesion was positively correlated with the maximal SUV ($r=0.632$, $p<0.01$) and the maximal LNR ($r=0.453$, $p<0.05$, Fig. 2). The number of $CD8^+$ T lymphocytes infiltrating the lesion was positively correlated with the maximal SUV ($r=0.540$, $p<0.01$) and the maximal LNR ($r=0.547$, $p<0.01$, Fig. 3). No significant correlations were found between the numbers of $CD68^+$ cells and $CD4^+$ T lymphocytes infiltrating the lesion and the $^{18}$F-FDG PET measurements.

All patients with cryptogenic organising pneumonia or organising pneumonia associated with collagen-vascular disease showed clinical improvement which was defined as an improvement in both CT findings and laboratory examinations. The three patients with drug-induced organising pneumonia responded to withdrawal of the implicated drug. In all patients with organising pneumonia, the median values of maximal SUV (0.65±0.18), mean SUV (0.38±0.16), maximal LNR (0.74±0.26) and mean LNR (0.61±0.21) were decreased with response to withdrawal of the implicated drug or corticosteroid therapy.

**Table 2.** $^{18}$ F-FDG PET measurements

| | Patients with organising pneumonia | Controls | *p* Value |
|---|---|---|---|
| Visual score | 4.70±0.10 | 1.60±0.10 | <0.0001 |
| Mean SUV | 1.00±0.02 | 0.31±0.01 | <0.0001 |
| Mean LNR | 1.49±0.06 | 0.48±0.02 | <0.0001 |
| Maximal SUV | 2.95±0.13 | 0.49±0.01 | <0.0001 |
| Maximal LNR | 4.44±0.30 | 0.75±0.03 | <0.0001 |

Values are expressed as mean ± standard deviation
*SUV* standardised uptake value, *LNR* lesion-to-normal lung tissue ratio

## Discussion

This study shows that a significant increase in $^{18}$F-FDG uptake occurs in the parenchymal lesions of patients with organising pneumonia. The enhanced $^{18}$F-FDG accumulation in patients with organising pneumonia is characterised by increased numbers of $CD45^+$ cells and $CD8^+$ T lymphocytes in the parenchymal lesion and is associated with the presence of air-space consolidation on PET/CT fused images. The significant correlations between the maximal SUV and various cellularities suggest that $^{18}$F-FDG accumulation in the lungs of these patients reflects the degree of disease activity.

Previous studies have shown the predictive value of the glucose metabolic rate in patients with pulmonary inflammation [16–19]. Inflammatory cells produce ATP at a level that is several times higher during activation, compared with at baseline. Inflammatory cells, like neutrophils and activated macrophages, at the site of inflammation also show increased $^{18}$F-FDG uptake. Using microautoradiography, Kubota et al. showed that newly formed granulation tissues around tumours and macrophages, which are concentrated in the outer zones surrounding the necrotic areas of tumours, significantly accumulated $^{18}$F-FDG in vitro [23]. The results of the present study appear to agree with these previous findings for pulmonary inflammation. However, no significant correlations were found between the numbers of $CD68^+$ cells and $CD4^+$ T lymphocytes infiltrating the lesion and the $^{18}$F-FDG PET measurements. This may be due to a different inflammatory response from that of outer zones surrounding the necrotic areas of tumours.

The mechanism of abnormal $^{18}$F-FDG uptake in patients with organising pneumonia is not clear. Histopathological examinations revealed that the numbers of $CD45^+$ cells and $CD8^+$ T lymphocytes in the parenchymal lesions were positively correlated with the maximal SUV, whereas the numbers of $CD68^+$ cells and $CD4^+$ T lymphocytes infiltrating the lesion were not significantly correlated with the maximal SUV. Pulmonary inflammation can be either acute or chronic, the former showing predominantly neutrophil infiltrates and a few eosinophils and monocytes, whereas $CD68^+$ cells are predominant in the latter [24]. $CD4^+$ and $CD8^+$ T lymphocytes, but not neutrophils, are also the dominant inflammatory cells in chronic inflammatory lesions, whereas neutrophils are attracted to acute phases. In our patients with organising pneumonia, the most active lesions are thought to be in the process of transition from acute to chronic pulmonary

**Table 3.** CT findings of organising pneumonia

| CT finding | No. (%) |
|---|---|
| Air-space consolidation | 18 (82) |
| Ground-glass attenuation | 17 (77) |
| Bronchial dilatation | 16 (73) |
| Band-like opacity | 11 (50) |
| Small nodular lesion | 10 (45) |
| Perilobular opacity | 6 (27) |

inflammation. These findings are in agreement with the concept that $^{18}$F-FDG uptake in inflammatory lesions is dependent on the presence of leucocytic or lymphocytic masses capable of binding the radioisotope.

The maximal SUV was associated with increased cellularity in the pathological specimens, the latter being characteristic of the active inflammatory process in organising pneumonia. In cases with organising pneumonia, the generalised signs of inflammation are frequently masked; however, our patients with organising pneumonia had higher CRP levels and WBCs than the control group. These findings support the use of the maximal SUV for staging active inflammation in organising pneumonia. A possible way to evaluate the contribution of the maximal SUV to staging of the disease would be to investigate the correlation between maximal SUV and clinical parameters, such as pulmonary function tests and CT findings. The increase in the number of inflammatory cells was not always paralleled by the CT patterns of organising pneumonia, as shown by the lack of any association between the maximal SUV and the five CT findings other

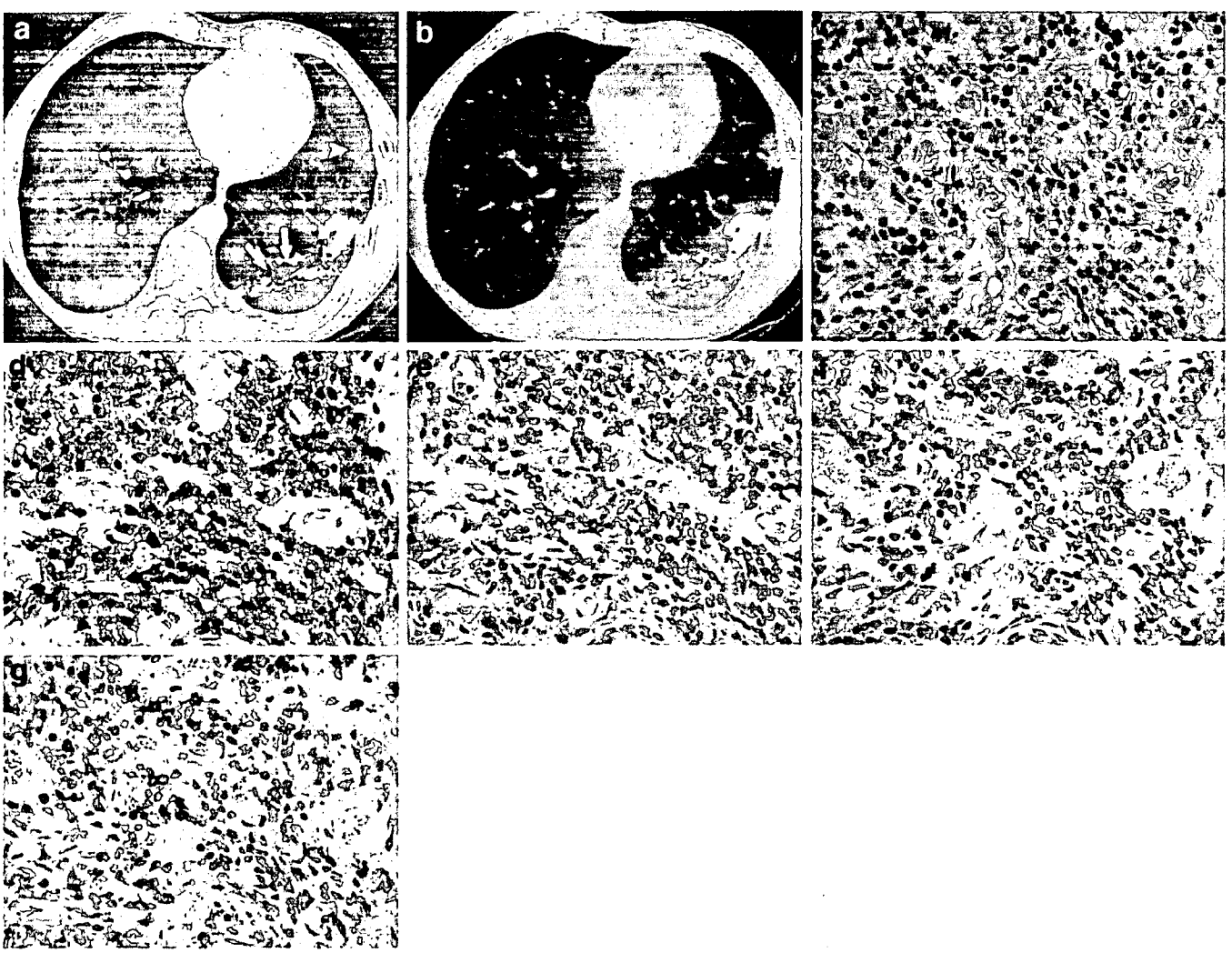


**Fig. 1. a.** Transverse CT scan through the lower lung lobes in a 54-year-old man with cryptogenic organising pneumonia. Air-space consolidation is visible in the periphery with areas of ground-glass attenuation and bronchial dilatation (*arrows*). A discrete patchy area of ground-glass attenuation is also visible (*arrowhead*). **b** Co-registered PET and CT image shows abnormal $^{18}$F-FDG uptake within the lesion. **c** Photomicrograph of the pathological specimen shows inflammatory cells in an excessive proliferation of granulation tissue (haematoxylin-eosin stain, original magnification ×200). **d–g** Immunostainings with monoclonal antibodies anti-CD45 (**d**), anti-CD68 (**e**), anti-CD4 (**f**) and anti-CD8 (**g**) show numerous positive cells within the lesion. Increased numbers of leucocytes ($CD45^+$ cells), macrophages ($CD68^+$ cells), CD4 T lymphocytes and CD8 T lymphocytes were seen (original magnification ×200)

**Table 4.** Results of cell counts in organising pneumonia

| Cell type | Cell count (cells/mm$^2$ ) |
|---|---|
| CD45+ cells, total leucocytes | 989.5±154.6 (688–1,268) |
| CD68+ cells, macrophages | 224.6±125.5 (70–489) |
| CD4+ cells, CD4+ T lymphocytes | 320.6±62.9 (201–470) |
| CD8+ cells, CD8+ T lymphocytes | 432.7±79.5 (332–580) |

Values are expressed as mean ± standard deviation (range)

than air-space consolidation. However, air-space consolidation, which was the most frequent finding in our study, was significantly associated with the maximal SUV, suggesting that the fusion of $^{18}$F-FDG PET and CT images may be useful for evaluating disease activity in patients with organising pneumonia.

Müller et al. [9] concluded that air-space consolidation identified on CT images was correlated with the presence of disease activity, as indicated by a histopathological analysis of specimens from patients with bronchiolitis obliterans with organising pneumonia (BOOP). Increased $^{18}$F-FDG accumulation was strongly correlated with disease activity in patients with BOOP [21]. As well as patients with organising pneumonia, which included a variety of inflammatory states of the lung in the present study, patients with infections, pneumoconiosis and tuberculosis can be expected to have positive $^{18}$F-FDG PET results [18]. While, increased $^{18}$F-FDG uptake during pulmonary inflammation is considered to be a non-specific finding, this measure often reflects disease activity or severity. Thus, the combination of $^{18}$F-FDG PET and CT images may be useful for indicating the regional active inflammation in patients with organising pneumonia, but not as a diagnostic test for the disease.

In our study, PET measurements of all patients were shown to be significantly depressed after recovery from organising pneumonia. Therefore, it can be postulated that evaluation of PET measurements may reflect disease activity in patients with organising pneumonia. Patients with organising pneumonia often receive steroids for extended periods, and $^{18}$F-FDG accumulation may be the sign of choice for monitoring disease activity [25]. However, steroid therapy may induce false negative results owing to hyperglycaemia while the underlying condition is still active. Further studies in this field, focussing on the progression of organising pneumonia and the efficacy of therapeutic protocols, are warranted.

One potential bias of the present study is that 18 of the patients with organising pneumonia underwent a transbronchial lung biopsy, whereas the others underwent an open lung biopsy. In open lung biopsies, the surgeon selects the lesion to be biopsied, and this may have influenced the results by exaggerating the differences in inflammatory cells between the two groups. However, if this was the case, the difference in inflammatory cells would be even greater between two better matched groups of patients, thus confirming that the findings of an enhanced inflammatory response in organising pneumonia are valid. Another potential bias of this study is that the co-registration of PET and CT images has a limited performance. Misregistration can be caused by body motion related to respiration, cardiovascular pulsation and patient movement, which is averaged over a relatively long time. Further studies using respiratory-gated PET/CT image fusion techniques to reduce the effect of misregistration are needed.

In conclusion, patients with organising pneumonia have an enhanced $^{18}$F-FDG accumulation within their lesions compared with normal subjects. The increased numbers of CD45$^+$ cells and CD8$^+$ T lymphocytes in parenchymal lesions are associated with air-space consolidation on PET/CT fused images, reflecting the degree of disease activity.

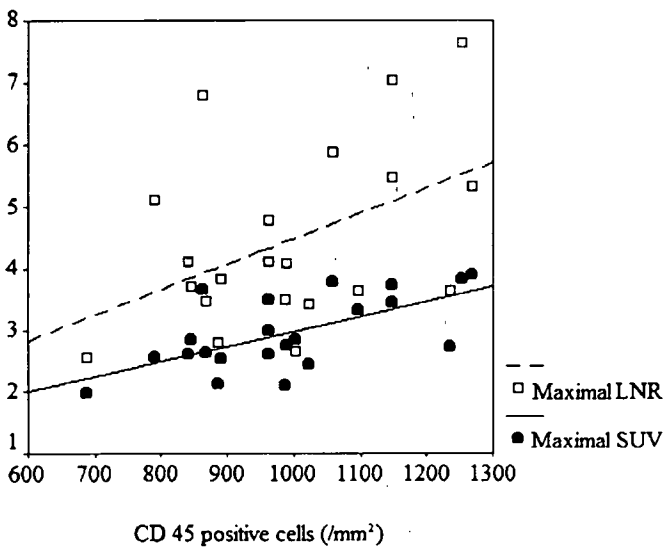


**Fig. 2.** Relationship between the number of total leucocytes (CD45$^+$ cells) and maximal SUV (•) or maximal LNR (□)

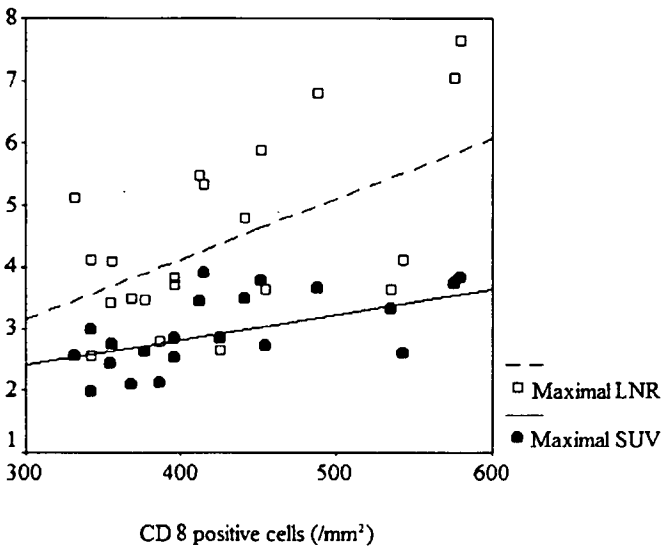


**Fig. 3.** Relationship between the number of CD8$^+$ T lymphocytes infiltrating the lesion and maximal SUV (•) or maximal LNR (□)

*Acknowledgements.* This work was supported in part by grants for Scientific Research Expenses for Health and Welfare Programs, No. 17–12, "The promotion and standardization of diagnostic accuracy in PET-CT imaging of lung cancer".

## References

1. Epler GR, Colby TV, McLoud TC, Carrington CB, Gaensler EA. Bronchiolitis obliterans organizing pneumonia. N Engl J Med 1985;312:152–158
2. Yousem SA, Lohr RH, Colby TV. Idiopathic bronchiolitis obliterans organizing pneumonia/cryptogenic organizing pneumonia with unfavorable outcome: pathologic predictors. Mod Pathol 1997;10:864–871
3. Cordier JF, Loire R, Brune J. Idiopathic bronchiolitis obliterans organizing pneumonia. Definition of characteristic clinical profiles in a series of 16 patients. Chest 1989;96:999–1004
4. Cordier JF. Organizing pneumonia. Thorax 2000;55:318–328
5. Siddiqui MT, Garrity ER, Husain AN. Bronchiolitis obliterans organizing pneumonia-like reactions: a nonspecific response or an atypical form of rejection or infection in lung allograft recipients? Hum Pathol 1996;27:714–719
6. Crestani B, Valeyre D, Roden S, Wallaert B, Dalphin JC, Cordier JF. Bronchiolitis obliterans organizing pneumonia syndrome primed by radiation therapy to the breast. The Groupe d'Etudes et de Recherche sur les Maladies Orphelines Pulmonaires (GERM"O"P). Am J Respir Crit Care Med 1998;158:1929–1935
7. Douglas WW, Tazelaar HD, Hartman TE, Hartman RP, Decker PA, Schroeder DR, et al. Polymyositis-dermatomyositis-associated interstitial lung disease. Am J Respir Crit Care Med 2001;164:1182–1185
8. Ohnishi H, Yokoyama A, Yasuhara Y, Watanabe A, Naka T, Hamada H, et al. Circulating KL-6 levels in patients with drug induced pneumonitis. Thorax 2003;58:872–875
9. Müller NL, Staples CA, Miller RR. Cryptogenic organizing pneumonia: CT findings in 14 patients. Am J Roentogenol 1990;154:983–987
10. Nishimura K, Itoh H. High-resolution computed tomographic features of bronchiolitis obliterans organizing pneumonia. Chest 1992;102:26–31
11. Oikonomou A, Hansell DM. Organizing pneumonia: the many morphological faces. Eur Radiol 2002;12:1486–1496
12. Murphy JM, Schnyder P, Verschakelen J, Leuenberger P, Flower CD. Linear opacities on HRCT in bronchiolitis obliterans organising pneumonia. Eur Radiol 1999;9:1813–1817
13. Ujita M, Renzoni EA, Veeraraghavan S, Well AU, Hansell DM. Organizing pneumonia: perilobular pattern at thin-section CT. Radiology 2004;232:757–761
14. Akira M, Sakatani M, Hara H. Thin-section CT findings in rheumatoid arthritis-associated lung disease: CT patterns and their courses. J Comput Assist Tomogr 1999;23:941–948
15. Kim SJ, Lee KS, Ryu YH, Yoon YC, Choe KO, Kim TS, et al. Reversed halo sign on high-resolution CT of cryptogenic organizing pneumonia: diagnostic implications. Am J Roentgenol 2003;180:1251–1254
16. Kapucu LO, Meltzer CC, Townsend DW. Fluorine-8-fluorodeoxyglucose uptake in pneumonia. J Nucl Med 1998;39:1267–1269
17. Lowe VJ, Hoffman JM, DeLong DM, Patz EF, Coleman RE. Semiquantitative and visual analysis of FDG-PET images in pulmonary abnormalities. J Nucl Med 1994;35:1771–1776
18. Alavi A, Gupta N, Alberini JL, Hickeson M, Adam LE, Bhargava P, et al. Positro emission tomography imaging in nonmalignant thoracic disorders. Semin Nucl Med 2002;32:293–321
19. Bakheet SM, Saleem M, Powe J, Amro AA, Larsson SG, Mahassin Z. F-18 fluorodeoxyglucose chest uptake in lung inflammation and infection. Clin Nucl Med 2000;25:273–278
20. Ichiya Y, Kuwabara Y, Sasaki M, Yoshida T, Akashi Y, Murayama S, et al. FDG-PET in infectious lesions: the detection and assessment of lesion activity. Ann Nucl Med 1996;10:185–191
21. Shin L, Katz DS, Yung E. Hypermetabolism on F-18 FDG PET of multiple pulmonary nodules resulting from bronchiolitis obliterans organizing pneumonia. Clin Nucl Med 2004;29: 654–656
22. Majeski EI, Harley RA, Bellum SC, London SD, London L. Differential role for T cells in the development of fibrotic lesions associated with reovirus 1/L-induced bronchiolitis obliterans organizing pneumonia versus acute respiratory distress syndrome. Am J Respir Cell Mol Biol 2003;28:208–217
23. Kubota R, Yamada S, Kubota K, Ishiwata K, Tamahashi N, Ido T. Intratumoral distribution of fluorine-18-fluorodeoxyglucose in vivo: high accumulation in macrophages and granulation tissues studied by microautoradiography. J Nucl Med 1992;33:1972–1980
24. Mukae H, Kadota J, Kohno S, Matsukura S, Hara K. Increase of activated T-cells in BAL fluid of Japanese patients with bronchiolitis obliterans organizing pneumonia and chronic eosinophilic pneumonia. Chest 1995;108:123–128
25. Oymak FS, Demirbas HM, Mavili E, Akgun H, Gulmez I, Demir R, et al. Bronchiolitis obliterans organizing pneumonia. Clinical and roentgenological features in 26 cases. Respiration 2005;72:254–262

# Glut-1 expression and enhanced glucose metabolism are associated with tumour grade in bone and soft tissue sarcomas: a prospective evaluation by [$^{18}$F]fluorodeoxyglucose positron emission tomography

Ukihide Tateishi[1,6], Umio Yamaguchi[2], Kunihiko Seki[3], Takashi Terauchi[4], Yasuaki Arai[1], Tadashi Hasegawa[5]

[1] Divisions of Diagnostic Radiology, National Cancer Center Hospital, 5-1-1, Tsukiji, Chuo-Ku, 104-0045 Tokyo, Japan
[2] Orthopedic Division, National Cancer Center Hospital, Tokyo, Japan
[3] Division of Clinical Pathology, National Cancer Center Hospital, Tokyo, Japan
[4] Division of Radiology, Research Center for Cancer Prevention and Screening, National Cancer Center, Tokyo, Japan
[5] Department of Clinical Pathology, Sapporo Medical University School of Medicine, Sapporo, Japan
[6] Division of Nuclear Medicine, National Cancer Center Hospital, 5-1-1, Tsukiji, Chuo-Ku, 104-0045 Tokyo, Japan

Received: 21 September 2005 / Accepted: 24 November 2005 / Published online: 28 February 2006


**Abstract.** *Purpose*: This study was conducted to investigate whether $^{18}$F-fluorodeoxyglucose (FDG) uptake, quantified by positron emission tomography (PET), correlates with histological variables including tumour grade, cell proliferation, cell cycle control integrity and glucose metabolism in patients with bone and soft tissue sarcomas.
*Methods*: Eighty-two patients clinically suspected of having a bone or soft tissue sarcoma underwent FDG PET within 1 week prior to operation and 63 patients (mean age 48 years, range 18–74 years) were enrolled in the complete analysis. We excluded 17 patients with pathologically confirmed benign tumours and two patients with uncontrolled diabetes or concomitant malignancy from data analysis. Maximum and average standardised uptake values (SUVs) of the primary lesion were compared with histological variables including tumour differentiation, the presence of necrosis, MIB-1 score, mitotic score, p53 overexpression, MIB-1 grade, mitotic grade and GLUT-1 expression.
*Results*: Significant correlations were found between maximal and mean SUVs and MIB-1 grade, mitotic grade, MIB-1 score, tumour differentiation and mitotic score. The mean and maximal SUVs were significantly higher in tumours with p53 overexpression than in those without p53 overexpression ($p<0.0001$). GLUT-1-positive tumours had significantly higher mean (6.5±4.2 vs 1.1± 0.2, $p=0.006$) and maximal SUVs (8.8±5.4 vs 1.7±0.5, $p=0.005$) than the GLUT-1-negative tumours. GLUT-1 intensity correlated positively with both mean ($r=0.500$, $p<0.0001$) and maximal SUVs ($r=0.509$, $p<0.0001$). Mu ltiple linear regression analysis showed a significant correlation between maximal SUV and MIB-1 grade ($p<0.0001$).
*Conclusion*: The enhanced glucose metabolism, as determined by SUV, is a strong index of tumour grade in bone and soft tissue sarcomas.

**Eur J Nucl Med Mol Imaging (2006) 33:683–691**
DOI 10.1007/s00259-005-0044-8

Ukihide Tateishi (✉)
Divisions of Diagnostic Radiology,
National Cancer Center Hospital,
5-1-1, Tsukiji, Chuo-Ku,
104-0045 Tokyo, Japan
e-mail: utateish@ncc.go.jp
Tel.: +81-3-35422511, Fax: +81-3-35423815

## Introduction

Bone and soft tissue sarcomas are rare malignant tumours which display great variation in histological type. While bone and soft tissue sarcomas are associated with a high mortality, better histological diagnosis and tumour grading are essential for correct treatment decisions and improved patient outcome [1]. Grading is performed according to a scheme based on tumour differentiation, amount of necrosis and number of mitotic figures [1, 2]. A Japanese grading system that uses the MIB-1 score instead of the mitotic score has recently been proposed as the most significant independent predictor of outcome [3, 4].

Optimal management of bone and soft tissue sarcomas depends on their anatomical site, size, growth pattern and tumour stage at the time of initial presentation, and the site, size, growth pattern, and tumour stage are best determined by cross-sectional imaging studies. Accurate imaging studies that provide additional information for tumour grading may be useful in the management of patients with

bone and soft tissue sarcomas [5]. Positron emission tomography with 2-[$^{18}$F]fluoro-2-deoxy-D-glucose (FDG PET) provides a means of non-invasive quantitative assessment of tumour glucose metabolism in vivo, and enhanced uptake reflects tumour aggressiveness in patients with bone and soft tissue sarcomas and has been used for diagnosis and grading of tumour type [6–10]. This suggests that FDG uptake may be one of the useful biomarkers for identifying aggressive tumours that require intensive treatment protocols and adequate evaluation of therapeutic response. However, there is a need to better understand the underlying mechanism of enhanced FDG uptake and the meaning of high uptake values in clinical settings.

The glucose transfer mediated by glucose transporter protein 1 (GLUT-1) plays a pivotal role in the development and malignant behaviour of cancer cells [11–16]. GLUT-1 belongs to the sugar transporter family and is the dominant protein expressed in cancer cells. It has been found to be overexpressed in cancer cells and to promote glucose metabolism and FDG accumulation [17–20]. However, GLUT-1 overexpression has never been clearly identified in bone and soft tissue sarcomas, and the relationship between GLUT-1 overexpression and FDG uptake or pathological background, including cellular proliferation activity and tumour grade, has never been systematically analysed. The pioneering study by Ito and co-workers [21] was designed to quantify GLUT-1 expression by human rhabdomyosarcoma cells, and the authors demonstrated that GLUT-1 accounted for a major part of the basal and insulin-stimulated glucose transport in vitro. The significance of GLUT-1 overexpression in bone and soft tissue sarcomas in vivo, however, has remained unexplored.

A prospective evaluation of tumour grade based on the FDG PET findings in patients with bone or soft tissue sarcomas has been reported [9, 10], but to the best of our knowledge the factors that influence FDG PET values, including histological variables, are still unknown. The aim of the present study was to identify the histological variables—including tumour grade, cell proliferation as measured by MIB-1 score, cell cycle control integrity as measured by immunohistochemical staining for p53 and overexpression of GLUT-1—that affect FDG PET values in patients with bone and soft tissue sarcomas.

## Materials and methods

*Patient eligibility*

Eligible patients were aged between 18 and 74 years and had a newly diagnosed tumour that was strongly suspected of being a bone or soft tissue sarcoma. Patients were questioned about the presence of three symptoms: induration, tenderness and numbness. The inclusion criteria for the performance status (PS) were PS 0 or PS 1. Exclusion criteria were active concomitant malignancy, clinical evidence of heart disease, uncontrolled diabetes, other severe complications and pregnancy or lactation. The study conformed to the Declaration of Helsinki, and informed written consent was obtained from each subject.

PET scanning was performed with dedicated PET scanners (ECAT ACCEL; Siemens/CTIMI, Knoxville, TN, USA) within 1 week prior to operation. The transverse field of view was 16.2 cm, and 47 image planes were produced. To correct for photon attenuation, a transmission scan was obtained prior to the emission scan with rotating $^{68}$Ge rod sources. Prior to PET study, the patients fasted for at least 6 h. All patients were tested for a normal glucose level (range 80–120 mg/dl) before PET scanning. Emission scans from the base of the head to toes were obtained starting 60–80 min after the intravenous administration of 300–370 MBq $^{18}$F-FDG. Images were reconstructed with attenuation-weighted ordered subset expectation maximisation with two iterations and eight subsets by using emission scans and reprojected attenuation maps as inputs.

CT scans were acquired using a stacked multislice acquisition protocol on a 16-detector row (Toshiba Medical Systems, Tokyo, Japan) CT scanner. A series of 5-mm-thick images were obtained with the following scan parameters: 120 kVp, 50–100 mA/rotation, 30–40 cm field of view and 512×512 matrix. The subjects were examined in the supine position, and no contrast material was used. All examinations were performed from the head to the toes. Images were reconstructed by using a standard algorithm. PET/CT fused images were made available and reviewed directly on the screen of the workstation (syngo; Siemens, Knoxville, TN, USA).

Images were reviewed in consensus by two board-certified radiologists who were blinded to clinical or radiological information, using hard-copy images in combination with a multimodality computer platform (syngo; Siemens, Knoxville, TN). The two radiologists reviewed all cases in which their interpretations were discrepant and reached a final decision by consensus. The initial

**Table 1.** Patient characteristics

| | |
|---|---|
| Age (yrs) | 47.5±2.0 |
| Male/female | 45 (71)/18 (29) |
| Mean size (cm) | 9.4±5.4 |
| 0–5 (cm) | 16 (25) |
| 5–10 (cm) | 19 (30) |
| 10– (cm) | 28 (45) |
| Type | |
| Skeletal tumour | 17 (27) |
| Extraskeletal tumour | 46 (73) |
| Distribution | |
| Extremities | 32 (51) |
| Trunk | 31 (49) |
| Diagnosis | |
| Pleomorphic MFH/undifferentiated high-grade pleomorphic sarcoma | 20 (33) |
| Ewing's sarcoma/PNET | 9 (15) |
| Synovial sarcoma | 8 (13) |
| Rhabdomyosarcoma | 5 (8) |
| Myxofibrosarcoma | 3 (5) |
| Extraskeletal myxoid chondrosarcoma | 3 (5) |
| Myxoid liposarcoma | 3 (5) |
| Extraskeletal osteosarcoma | 2 (3) |
| Angiosarcoma | 2 (3) |
| Well-differentiated liposarcoma | 2 (3) |
| Fibrosarcoma | 2 (3) |
| Dedifferentiated liposarcoma | 1 (2) |

Data are presented as mean±standard deviation (SD). The numbers in parentheses are percentages

*MFH* malignant fibrous histiocytoma, *PNET* primitive neuroectodermal tumour

review of the attenuation-corrected PET images was performed in transaxial, coronal and sagittal planes. Visual analysis was used, and lesions with abnormal FDG uptake were recorded. Abnormal FDG uptake was defined as uptake higher than the background activity in the soft tissue. Lesions with abnormal FDG uptake were confirmed on PET/CT fused images, and their likely anatomical location was recorded. For semiquantitative analysis of the FDG uptake, regions of interest (ROIs) were manually positioned over the tumour in the transmission image. The ROIs placed on the lesions encompassed all pixels that had uptake values greater than 90% of the maximum uptake. When the tumour was extensively heterogeneous, the ROIs were set to cover all the components of the tumour. After correction for radioactive decay, we analysed the ROIs by computing the standardised uptake value (SUV), and both the maximum pixel value within the ROI (maximal SUV) and the mean SUV were recorded. The average values of mean SUV and maximal SUV for each tumour obtained by the IRSAC reconstruction method were calculated along with SD statistics.

*Histology*

Pathology specimens of all the patients' tumours were obtained by incisional biopsy after the imaging studies, and histological slides were prepared for diagnosis by two expert pathologists. Whenever necessary, immunohistochemical staining was carried out to confirm the diagnosis or tumour type according to the WHO classification system [1]. Mitotic counts in ten high-power fields were determined and classified into three groups. Tumour specimens were immunostained with the antibody Ki-67 (clone MIB-1; DakoCytomation; diluted 1:100 and autoclaved) and the Ki-67 (MIB-1) labelling index (LI) was estimated by calculating the percentage of Ki-67-positive cell nuclei among 1,000 tumour cells in the region of the tumour in which the greatest density of Ki-67 staining was observed under a light microscope. Both the MIB-1 grade (the Japanese grading system) and the mitotic grade (the modified French system) are three-grade systems obtained by summing the scores of tumour differentiation, tumour necrosis and the MIB-1 score or mitotic score, each of which is given a score of 0, 1, 2 or 3 [4, 22]. The tumour differentiation score according to histological type was modified slightly from the French system [22]. The mitotic figures were counted on routine haematoxylin and eosin-stained sections. The areas selected for cell counting were in the most mitotically active parts of the tumours, usually located at the periphery. The mitotic score was obtained by counting the number of mitotic figures in ten consecutive high-power fields. The MIB-1 score was estimated by calculating the percentage of MIB-1-positive cell nuclei among 1,000 tumour cells in the region of the tumour with the greatest density of staining, which in most instances corresponded to the area with the highest mitotic activity. In this study, the histological grade of the tumour was determined by using a three-grade system in which tumour differentiation, tumour necrosis and MIB-1 LI were each given a score of 0, 1, 2, or 3 and the scores were added together [3, 4]. Lesions with MIB-1 LIs of 0–9%, 10–29%, and greater than 30% were assigned MIB-1 scores of 1, 2 and 3, respectively. The three separate scores were added together to produce a combined grade: lesions whose total score was 2 or 3 were classified as grade 1, those whose total score was 4 or 5, as grade 2, and those whose total score

**Table 2.** Pathological variables and SUVs

| | No. | Maximal SUV | *p* Value | Mean SUV | *p* Value |
|---|---|---|---|---|---|
| MIB-1 grade* | | | <0.0001 | | <0.0001 |
| 1 | 13 (21) | 2.6±1.6 | | 1.7±1.1 | |
| 2 | 11 (17) | 5.2±3.2 | | 3.6±2.8 | |
| 3 | 39 (62) | 11.1±5.0 | | 8.2±3.8 | |
| Mitotic grade* | | | <0.0001 | | <0.0001 |
| 1 | 15 (24) | 3.3±2.6 | | 2.5±2.6 | |
| 2 | 11 (17) | 7.7±5.4 | | 4.8±3.4 | |
| 3 | 37 (59) | 10.5±5.2 | | 7.9±4.0 | |
| Differentiation* | | | <0.0001 | | <0.0001 |
| 1 | 8 (13) | 3.3±2.3 | | 2.2±1.6 | |
| 2 | 13 (21) | 4.1±3.3 | | 2.8±2.7 | |
| 3 | 42 (67) | 10.5±5.2 | | 7.8±4.0 | |
| Necrosis | | | 0.539 | | 0.366 |
| 0 | 49 (78) | 8.1±6.0 | | 5.8±4.5 | |
| 1 | 9 (14) | 9.9±4.3 | | 7.6±3.7 | |
| 2 | 5 (8) | 7.6±2.6 | | 5.6±3.2 | |
| MIB-1 score* | | | <0.0001 | | <0.0001 |
| 1 | 16 (25) | 2.8±1.7 | | 1.8±1.1 | |
| 2 | 9 (14) | 7.2±4.3 | | 5.0±3.4 | |
| 3 | 38 (60) | 10.9±5.1 | | 8.1±3.9 | |
| Mitotic score* | | | 0.006 | | 0.002 |
| 0 | 2 (3) | 6.5±7.1 | | 3.1±2.9 | |
| 1 | 25 (40) | 5.9±4.9 | | 4.3±4.0 | |
| 2 | 6 (10) | 6.8±3.5 | | 4.6±2.2 | |
| 3 | 30 (48) | 10.7±3.5 | | 8.0±4.2 | |

Data are presented as mean±SD. The numbers in parentheses are percentages

*Significant differences ($p<0.05$) were found between groups by the Kruskal-Wallis test. Significant differences were found for MIB-1 grade 1 vs 3, MIB-1 grade 2 vs 3, mitotic grade 1 vs 2, mitotic grade 1 vs 3, mitotic grade 2 vs 3, differentiation 1 vs 3, differentiation 2 vs 3, MIB-1 score 1 vs 3, MIB-1 score 2 vs 3, mitotic score 0 vs 2, mitotic score 0 vs 3, mitotic score 1 vs 2, and mitotic score 1 vs 3

was 6, 7 or 8, as grade 3. Grade 3 tumours were classified as "high grade", and grade 1 and 2 tumours as "low grade". According to this MIB-1 system, tumours were assigned grades 1–3.

A mouse monoclonal antibody (clone DO7; Dako; diluted 1:1,000) was used to immunostain tumour specimens for the p53 epitope located between amino acids 19 and 26 of wild-type and mutant human p53 proteins. p53 overexpression was defined as present when more than 20% of the tumour cells contained nuclei that were immunostained. For GLUT-1, the primary antibody applied was an affinity-purified goat polyclonal antibody (A3536; Dako; diluted 1:500). The intensity of GLUT-1 staining was quantified with regard to the percentage of cells stained. Intensity of GLUT-1 staining was scored as 0 (0%), 1 (1–9%), 2 (10–29%) or 3 (greater than 30%). The p53 overexpression and intensity of GLUT-1 staining were reviewed by two expert pathologists unaware of the clinical information. The final determination of p53 overexpression and intensity of GLUT-1 staining was made by consensus.

*Statistical analysis*

The demographic variables and imaging characteristics of patients were analysed for statistically significant differences using the $\chi^2$ or Fisher's exact test for categorised variables. A comparison of differences was performed by the two-sample $t$ test. The Kruskal-Wallis test was used to evaluate the differences between the groups defined by each grade. The predictive performance of SUV was evaluated by receiver operating characteristic (ROC) analysis, and areas under the curve were represented by the $A_z$ values. The correlations between pathological parameters and SUV were analysed by Pearson correlation coefficient analysis and multiple linear regression analysis. A $p$ value of $<0.05$ was considered to indicate a statistically significant difference.

## Results

Eighty-two patients clinically suspected of having a bone or soft tissue sarcoma underwent FDG PET, but 19 failed to meet the criteria. One patient had active concomitant malignancy and heart failure. In another patient, the diabetes was uncontrolled before randomisation. Seventeen patients were excluded because they had benign bone or soft tissue lesions: haemangioma ($n$=4), inflammatory change ($n$=4), neurinoma ($n$=3), haematoma ($n$=2), lipoma ($n$=1), fibrous dysplasia ($n$=1), enchondroma ($n$=1) and giant cell tumour of the tendon sheath ($n$=1). The remaining 63 patients were the subjects of the complete analysis.

The characteristics of the patients are shown in Table 1. The median age at the time of presentation was 53 years, and seven patients were under 20 years of age. The tumour was located in an extremity in 24 patients and in the trunk in 36 patients. The median tumour size was 9.4 cm, and tumour size ranged from 1.2 to 24.0 cm. Patients in each tumour grade were similar with regard to age, gender, size and tumour location. No significant differences in mean and maximal SUVs were observed between the distribution of the tumour (trunk versus extremities) and tumour size. No significant correlation was observed between tumour size and the mean or maximal SUV. There were 46 extraskeletal tumours and 17 skeletal tumours; there were

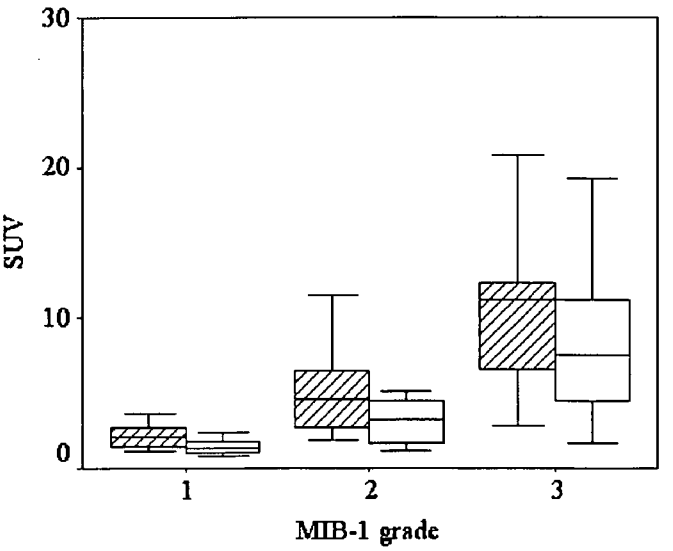


**Fig. 1.** The relationship between MIB-1 grade and the maximal (*hatched bars*) and mean SUV (*open bars*). Using the Kruskal Wallis test, significant differences were found between MIB-1 grades 1 and 3 and between MIB-1 grades 2 and 3 with respect to both maximal and mean SUV ($p$<0.05)

no significant differences in mean and maximal SUVs between extraskeletal and skeletal tumours.

Kruskal-Wallis analysis showed significantly different variance in mean and maximal SUV between groups classified by MIB-1 grade ($p$<0.0001), mitotic grade ($p$<0.0001), differentiation ($p$<0.0001) and MIB-1 score ($p$<0.0001, Table 2). Patients with high-grade tumours had significantly higher mean and maximal SUVs than those with low-grade tumours ($p$<0.05, Table 2, Figs. 1 and 2). The ROC analyses to predict high-grade tumours revealed $A_z$ values for mean and maximal SUV of 0.926 (95%CI

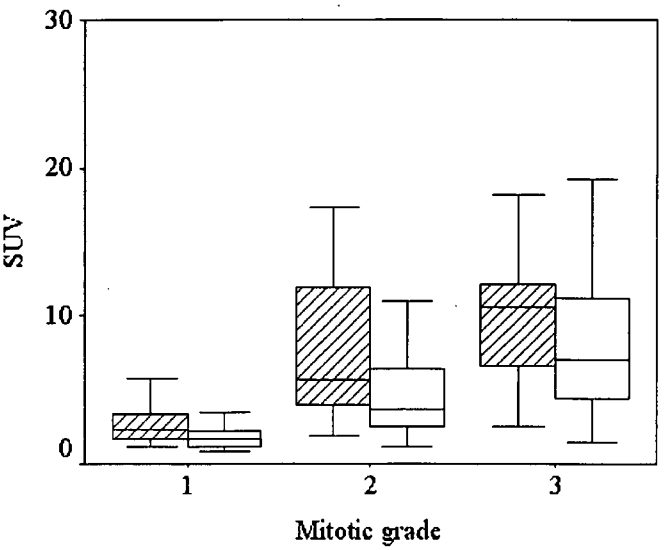


**Fig. 2.** The relationship between mitotic grade and the maximal (*hatched bars*) and mean SUV (*open bars*). Using the Kruskal Wallis test, significant differences were found between mitotic grades 1 and 3 and between mitotic grades 2 and 3 with respect to both maximal and mean SUV ($p$<0.05)

0.860–0.992) and 0.919 (0.847–0.991), respectively, by MIB-1 grade, and 0.817 (0.698–0.935) and 0.842 (0.740–0.944), respectively, by mitotic grade.

Visual analysis showed that 59 tumours were positive on FDG PET. All visually negative tumours were MIB-1 grade 1 and mitotic grade 1 ($n$=4). However, nine tumours with MIB-1 grade 1 and 11 tumours with mitotic grade 1 were visually positive on FDG PET.

It was found that in 49.2% of patients, tumours showed p53 overexpression (Table 3). The mean and maximal SUVs were significantly higher in tumours with p53 overexpression than in those without p53 overexpression ($p$<0.0001, Table 3, Fig. 3). The ROC analysis to predict tumours with p53 overexpression showed $A_z$ values for mean and maximal SUV of 0.866 (0.776–0.957) and 0.876 (0.787–0.964), respectively.

GLUT-1 was expressed in 92.0% of tumours (Fig. 4). Along with GLUT-1 expression in tumour cells, specific GLUT-1 expression was also found in erythrocytes, perineurium of the peripheral nerves and lymphocytes in the germinal zone. GLUT-1 immunostaining was absent in five tumours: four well-differentiated liposarcomas and one clear cell chondrosarcoma. GLUT-1-positive tumours had significantly higher mean (6.5±4.2 vs 1.1±0.2, $p$=0.006) and maximal SUVs (8.8±5.4 vs 1.7±0.5, $p$=0.005) than the GLUT-1-negative tumours (Table 4, Fig. 5). GLUT-1 intensity correlated positively with both mean ($r$=0.500, $p$<0.0001) and maximal SUVs ($r$=0.509, $p$<0.0001). There were significant associations between GLUT-1 intensity and MIB-1 grade ($p$<0.0001), mitotic grade ($p$<0.0001), differentiation ($p$<0.0001), MIB-1 score ($p$<0.0001) and mitotic score ($p$<0.0001, Table 5).

The univariate analysis revealed positive correlations between both mean and maximal SUVs and mitotic grade, MIB-1 grade, mitotic score and tumour differentiation, but the correlation between both mean and maximal SUVs and the degree of necrosis was not significant (Table 6). Multiple linear regression analysis showed a significant correlation between maximal SUV and MIB-1 grade ($p$<0.0001).

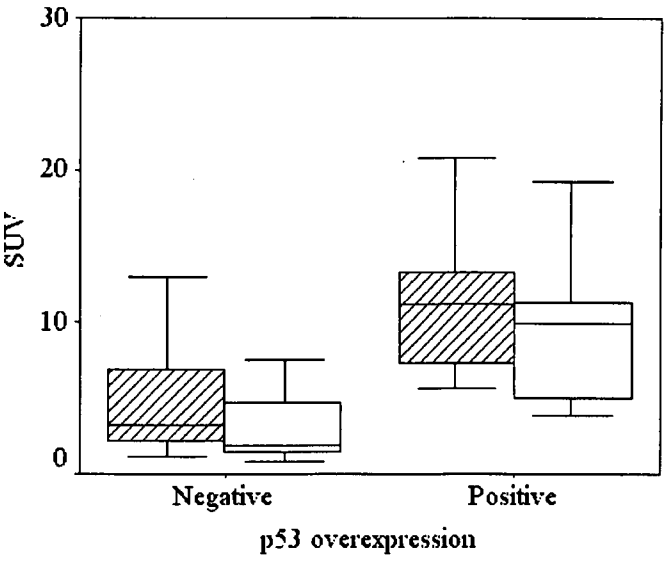


**Fig. 3.** The relationship between the presence or absence of p53 overexpression and the maximal (*hatched bars*) and mean SUV (*open bars*). A significant difference was found in both groups ($p$<0.0001)

**Table 3.** p53 overexpression, SUVs and pathological variables

| | Overexpression (+) | Overexpression (−) | $p$ Value |
|---|---|---|---|
| No. | 31 (49) | 32 (51) | |
| Maximal SUV* | 11.7±5.1 | 5.0±3.7 | <0.0001 |
| Mean SUV* | 8.8±3.7 | 3.5±3.1 | <0.0001 |
| MIB-1 grade** | | | <0.0001 |
| 1 | 0 | 13 (21) | |
| 2 | 1 (2) | 10 (16) | |
| 3 | 30 (48) | 9 (14) | |
| Mitotic grade** | | | <0.0001 |
| 1 | 1 (2) | 14 (22) | |
| 2 | 2 (3) | 9 (14) | |
| 3 | 28 (44) | 9 (14) | |
| Differentiation** | | | <0.0001 |
| 1 | 1 (2) | 7 (11) | |
| 2 | 1 (2) | 12 (19) | |
| 3 | 29 (46) | 13 (21) | |
| Necrosis** | | | 0.006 |
| 0 | 19 (30) | 30 (48) | |
| 1 | 7 (11) | 2 (3) | |
| 2 | 5 (8) | 0 | |
| MIB-1 score** | | | <0.0001 |
| 1 | 0 | 16 (25) | |
| 2 | 2 (3) | 7 (11) | |
| 3 | 29 (46) | 9 (14) | |
| Mitotic score** | | | <0.0001 |
| 0 | 0 | 2 (3) | |
| 1 | 6 (10) | 19 (30) | |
| 2 | 2 (3) | 4 (6) | |
| 3 | 23 (37) | 7 (11) | |

Data are presented as mean±SD. The numbers in parentheses are percentages

*Significant difference was found between two groups by two-sample $t$ test; **significant difference was found between two groups by Fisher's exact test

## Discussion

The results of this study showed that, in patients with bone and soft tissue sarcoma, FDG uptake was significantly correlated with MIB-1 grade, mitotic grade, MIB-1 score, mitotic score and tumour differentiation. The enhanced metabolic response in patients with bone and soft tissue sarcoma is characterised by both increased GLUT-1 staining intensity and p53 overexpression.

Previous studies have shown that increased FDG uptake has a significant correlation with tumour grade in patients with bone and soft tissue sarcomas and that the maximal SUV quantified by FDG uptake is the most reliable predictor of high-grade bone and soft tissue sarcoma [6, 7].

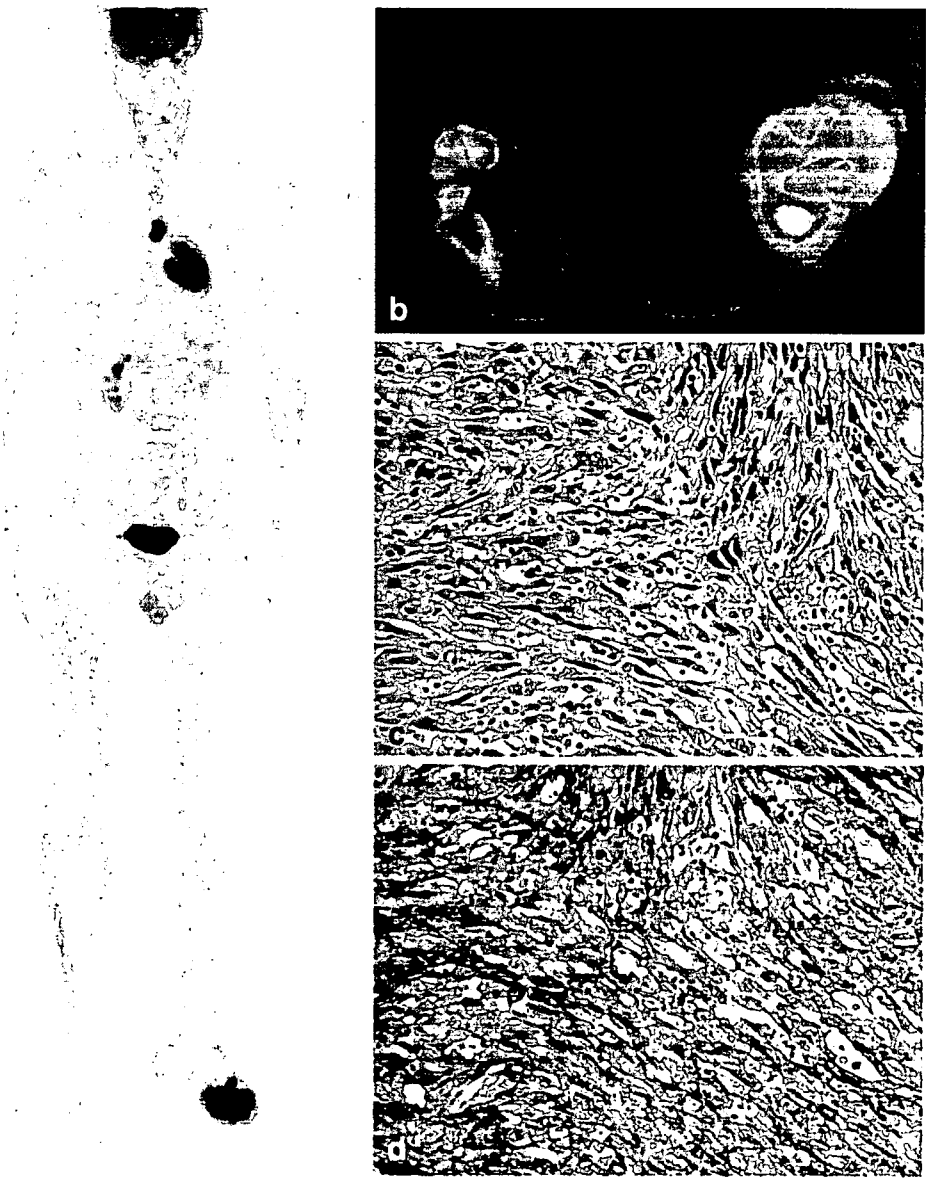


**Fig. 4.** Pleomorphic malignant fibrous histiocytoma (MFH)/ undifferentiated high-grade pleomorphic sarcoma. **a** PET. Coronal maximum intensity projection image of a 33-year-old man with increased accumulation in the primary tumour of the left foot and sternal metastasis. **b** Co-registered PET and CT images. The tumour shows a maximal SUV of 14.6 and a mean SUV of 11.6. **c, d** Paraffin sections obtained from the tumour demonstrate tumour cells with marked nuclear pleomorphism (**c** haematoxylin-eosin stain) and overexpression of GLUT-1 (**d** GLUT-1 intensity: 3). Tumour shows high-grade features, with MIB-1 grade 3, mitotic grade 3, differentiation 3, necrosis 2, MIB-1 score 3, mitotic score 3 and overexpression of p53

Overexpression of GLUT-1 is the common mediator of glucose uptake in neoplastic cells that supports increased glucose metabolism and promotes neoplastic cells in hypoxic areas. The present study, by demonstrating that there is amplification of GLUT-1 expression when FDG accumulation by tumours increases, builds upon the recent findings of Folpe et al., who suggested a significant correlation between FDG uptake and proliferative activity and cell cycle control integrity in bone and soft tissue sarcomas [8]. The results of the present study may appear to be consistent with the previous studies showing a relationship between glucose metabolism and tumour grade in bone and soft tissue sarcoma [9]. However, most of these studies reviewed cases of bone and soft tissue sarcomas by means of retrospective analyses, and lacked evaluation of GLUT-1 expression [10]. Our study goes beyond earlier observations by showing that FDG uptake is associated with tumour grade as well as with GLUT-1 expression.

**Table 4.** GLUT-1 intensity and SUV

| GLUT-1 intensity | No. | Mean SUV | Maximal SUV |
|---|---|---|---|
| 0 | 5 (8) | 1.1±0.2 | 1.7±0.5 |
| 1 | 4 (6) | 2.6±1.3 | 3.9±1.7 |
| 2 | 16 (25) | 4.8±3.5 | 6.6±4.2 |
| 3 | 38 (60) | 7.6±4.2 | 10.3±5.6 |

Data are presented as mean±SD. The numbers in parentheses are percentages

Significant differences were found in GLUT-1 intensity 0 vs 1, 0 vs 2, 0 vs 3, 1 vs 3 and 2 vs 3 ($p<0.05$)

Among the factors relevant to tumour grading, MIB-1 grade appeared to contribute most significantly to the enhanced glucose metabolism in patients with bone and soft tissue sarcoma. MIB-1 expression, which is confined

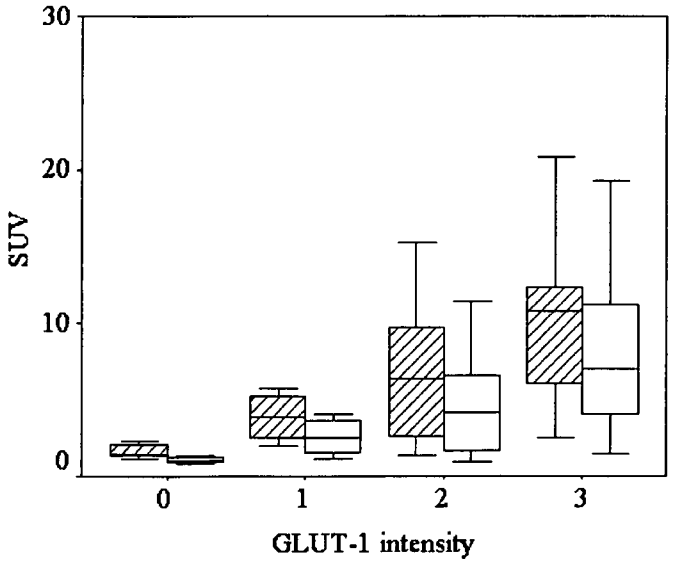


**Fig. 5.** The relationship between GLUT-1 intensity and the maximal (*hatched bars*) and mean SUV (*open bars*). Using the Kruskal Wallis test, significant differences were found between GLUT-1 intensities 0 and 1, GLUT-1 intensities 0 and 2, GLUT-1 intensities 0 and 3, GLUT-1 intensities 1 and 3, and GLUT-1 intensities 2 and 3 with respect to both maximal and mean SUV ($p<0.05$)

to the late $G_1$, S, M and $G_2$ phases of the cell cycle, has traditionally been considered an independent predictor of poor outcome [3]. As pointed out in our previous study, it is conceivable that the MIB-1 grading system has better predictive value than the MIB-1 score and standard grading or staging in the main histological types of soft tissue sarcoma [4]. Therefore, FDG, which reflects proliferative activity, has the potential to stage bone and soft tissue sarcomas. The recent observation of a relationship between enhanced glucose metabolism and the MIB-1 labelling index supports this observation [8]. On the other hand, our results indicate that it is also possible that a more relevant correlation exists between enhanced glucose metabolism and MIB-1 grade.

Our observation of a significant association between enhanced glucose metabolism and p53 overexpression appears to be consistent with the report by Folpe et al., who demonstrated correlations between SUVs and measures of cell cycle control integrity [8]. However, in comparison with previous studies, our study had significant differences that may have influenced our results. The incidence of p53 overexpression in soft tissue sarcoma has been reported to range from 9% to 41% [23–25]. In contrast, we found p53 overexpression in 49% of patients with grade 2 or 3

**Table 5.** GLUT-1 intensity and pathological variables

| | GLUT-1 intensity | | | | *p* Value |
|---|---|---|---|---|---|
| | 0 | 1 | 2 | 3 | |
| MIB-1 grade* | | | | | <0.0001 |
| 1 | 5 (8) | 2 (3) | 4 (5) | 2 (3) | |
| 2 | 0 | 2 (3) | 4 (5) | 5 (8) | |
| 3 | 0 | 0 | 8 (13) | 31 (49) | |
| Mitotic grade* | | | | | <0.0001 |
| 1 | 5 (8) | 2 (3) | 5 (8) | 3 (5) | |
| 2 | 0 | 2 (3) | 4 (5) | 5 (8) | |
| 3 | 0 | 0 | 7 (11) | 30 (48) | |
| Differentiation* | | | | | <0.0001 |
| 1 | 4 (6) | 0 | 1 (2) | 3 (5) | |
| 2 | 1 (2) | 3 (5) | 6 (10) | 3 (5) | |
| 3 | 0 | 1 (2) | 9 (14) | 32 (51) | |
| Necrosis | | | | | 0.719 |
| 0 | 5 (8) | 4 (6) | 13 (21) | 27 (43) | |
| 1 | 0 | 0 | 2 (3) | 7 (11) | |
| 2 | 0 | 0 | 1 (2) | 4 (6) | |
| MIB-1 score* | | | | | <0.0001 |
| 1 | 5 (8) | 2 (3) | 7 (11) | 2 (3) | |
| 2 | 0 | 2 (3) | 2 (3) | 5 (8) | |
| 3 | 0 | 0 | 7 (11) | 31 (49) | |
| Mitotic score* | | | | | 0.009 |
| 0 | 1 (2) | 0 | 0 | 1 (2) | |
| 1 | 4 (6) | 3 (5) | 8 (13) | 10 (16) | |
| 2 | 0 | 1 (2) | 3 (5) | 2 (3) | |
| 3 | 0 | 0 | 5 (8) | 25 (40) | |

The numbers in parentheses are percentages

*Significant difference was found between two groups by Fisher's exact test

**Table 6.** Correlations between SUV and pathological variables

| | Maximal SUV | *p* Value | Mean SUV | *p* Value |
|---|---|---|---|---|
| MIB-1 grade | 0.649 | <0.0001 | 0.65 | <0.0001 |
| Mitotic grade | 0.534 | <0.0001 | 0.547 | <0.0001 |
| Differentiation | 0.544 | <0.0001 | 0.547 | <0.0001 |
| Necrosis | 0.035 | 0.787 | 0.057 | 0.657 |
| MIB-1 score | 0.626 | <0.0001 | 0.64 | <0.0001 |
| Mitotic score | 0.402 | <0.001 | 0.428 | <0.0001 |

tumours. This observation is in line with the results of the study by Folpe et al., who demonstrated p53 overexpression in 45% of patients with bone and soft tissue sarcoma, among whom the proportion with grade 2 or 3 tumours was 65% [8]. However, in addition to the higher proportion of patients with p53 overexpression in our study, there were other potentially relevant differences in patient populations.

Like every imaging study, our study had certain limitations. First, the degree of necrosis within the tumour was not paralleled by enhanced glucose metabolism. This suggests that the presence of microscopic necrosis itself may not play a significant role in FDG accumulation. However, when imaging studies of hypoxia, which is strictly linked to tumour necrosis, are considered together, the presence of necrosis is found to be associated with FDG measurements. In addition, there may be inflammatory influences on FDG accumulation, because necrosis within tumour is often associated with macrophage activation. Second, there were five GLUT-1-negative tumours with FDG accumulation. In fact, many glucose transporters exist and are associated with various kinds of malignant tumour [26]. It is possible that GLUT-1-negative tumours would have been positive for other transporters, such as GLUT-3 or GLUT-4. Third, the eight patients with benign tumours were not included in the complete analysis, and this may have influenced the results by exaggerating the high metabolic rates in bone and soft tissue sarcomas. However, enhanced glucose metabolism is also observed in benign bone and soft tissue tumours, including giant cell tumours, because of their proliferative activity and the productive potential of the intercellular matrix [27–29]. Finally, the different uptake time in each patient may have been a source of bias; delayed scan may cause an increase in maximal SUV, such that the actual SUV may have been overestimated in our study.

In conclusion, patients with bone and soft tissue sarcomas have an enhanced glucose metabolism which is correlated with tumour grade. The enhanced glucose metabolism is also associated with increased GLUT-1 staining intensity and with p53 overexpression by the tumour, suggesting a role for this enhanced metabolic response in the evaluation prior to therapy.

*Acknowledgements.* We thank Hiromitsu Daisaki, Takeshi Murano, and Masashi Suzuki for helping to develop the criteria for the technical quality of the FDG PET/CT imaging; Tetsuo Maeda and Mototaka Miyake for assisting with the literature search; and Yasuo Beppu, Hirokazu Chuman, Akira Kawai and Fumihiko Nakatani for assisting with clinical information. This work was supported in part by grants from Scientific Research Expenses for Health and Welfare Programs, No. 17-12, the promotion and standardization of diagnostic accuracy in PET/CT imaging and BMS Freedom to Discovery Grant. This work was also supported by Travel Grant of the Princess Takamatsu Cancer Research Fund.

## References

1. Weiss SW, Goldblum JR Enzinger and Weiss's soft tissue tumors. 4th edn. St. Louis: Mosby, 2001
2. Costa J, Wesley RA, Glastein E, Rosenberg SA The grading of soft tissue sarcomas. Results of a clinicopathologic correlation in a series of 163 cases. Cancer 1984;53:530–541
3. Hasegawa T, Yamamoto S, Yokoyama R, Umeda T, Matsuno Y, Hirohashi S Prognostic significance of grading and staging systems using MIB-1 score in adult patients with soft tissue sarcoma of the extremities and trunk. Cancer 2002;95:843–851
4. Hasegawa T, Yamamoto S, Nojima T, Hirose T, Nikaido T, Yamashiro K, et al. Validity and reproducibility of histologic diagnosis and grading for adult soft-tissue sarcomas. Hum Pathol 2002;33:111–115
5. Bredella MA, Caputo GR, Steinbach LS Value of FDG positron emission tomography in conjunction with MR imaging for evaluating therapy response in patients with musculoskeletal sarcomas. AJR Am J Roentogenol 2002;179:1145–1150
6. Nieweg OE, Pruim J, van Ginkel RJ, Hoekstra HJ, Paans AM, Molenaar WM, et al. Fluorine-18-fluorodeoxyglucose PET imaging of soft-tissue sarcoma. J Nucl Med 1996;37:257–261
7. Eary JF, Conrad EU, Bruckner JD, Folpe A, Hunt KJ, Mankoff DA, et al. Quantitative [F-18]fluorodeoxyglucose positron emission tomography in pretreatment and grading of sarcoma. Clin Cancer Res 1998;4:1215–1220
8. Folpe AL, Lyles RH, Sprouse JT, Conrad EU 3rd, Eary JF (F-18) fluorodeoxyglucose positron emission tomography as a predictor of pathologic grade and other prognostic variables in bone and soft tissue sarcoma. Clin Cancer Res 2000;6:1279–1287
9. Ioannidis JP, Lau J $^{18}$F-FDG PET for the diagnosis of soft-tissue sarcoma: a meta-analysis. J Nucl Med 2003;44:717–724
10. Bastiaannet E, Groen H, Jager PL, Cobben DC, van der Graaf WT, Vaalburg W, et al. The value of FDG-PET in the detection, grading and response to therapy of soft tissue and bone sarcomas; a systematic review and meta-analysis. Cancer Treat Rev 2004;30:83–101
11. Chung JK, Lee YJ, Kim SK, Jeong JM, Lee DS, Lee MC Comparison of [$^{18}$F]fluorodeoxyglucose uptake with glucose transporter-1 expression and proliferation rate in human glioma and non-small-cell lung cancer. Nucl Med Commun 2004;25 (1):11–17
12. Mamede M, Higashi T, Kitaichi M, Ishizu K, Ishimori T, Nakamoto Y, Yanagihara K, Li M, Tanaka F, Wada H, Manabe T, Saga T [$^{18}$F]FDG uptake and PCNA, Glut-1, and hexokinase-II expressions in cancers and inflammatory lesions of the lung. Neoplasia 2005;7:369–379
13. Brown RS, Leung JY, Fisher SJ, Frey KA, Ethier SP, Wahl RL Intratumoral distribution of tritiated-FDG in breast carcinoma: correlation between Glut-1 expression and FDG uptake. J Nucl Med 1996;37(6):1042–1047

14. Reske SN, Grillenberger KG, Glatting G, Port M, Hildebrandt M, Gansauge F, et al. Overexpression of glucose transporter 1 and increased FDG uptake in pancreatic carcinoma. J Nucl Med 1997;38:1344–1348
15. Higashi T, Tamaki N, Honda T, Torizuka T, Kimura T, Inokuma T, et al. Expression of glucose transporters in human pancreatic tumors compared with increased FDG accumulation in PET study. J Nucl Med 1997;38:1337–1344
16. Higashi T, Saga T, Nakamoto Y, Ishimori T, Mamede MH, Wada M, et al. Relationship between retention index in dual-phase $^{18}$F-FDG PET, and hexokinase-II and glucose transporter-1 expression in pancreatic cancer. J Nucl Med 2002;43: 173–180
17. Kunkel M, Reichert TE, Benz P, Lehr HA, Jeong JH, Wieand S, et al. Overexpression of Glut-1 and increased glucose metabolism in tumors are associated with a poor prognosis in patients with oral squamous cell carcinoma. Cancer 2003;97: 1015–1024
18. Kato H, Takita J, Miyazaki T, Nakajima M, Fukai Y, Masuda N, et al. Correlation of 18-F-fluorodeoxyglucose (FDG) accumulation with glucose transporter (Glut-1) expression in esophageal squamous cell carcinoma. Anticancer Res 2003;23: 3263–3272
19. Yen TC, See LC, Lai CH, Yah-Huei CW, Ng KK, Ma SY, et al. $^{18}$F-FDG uptake in squamous cell carcinoma of the cervix is correlated with glucose transporter 1 expression. J Nucl Med 2004;45:22–29
20. Kurokawa T, Yoshida Y, Kawahara K, Tsuchida T, Okazawa H, Fujibayashi Y, et al. Expression of GLUT-1 glucose transfer, cellular proliferation activity and grade of tumor correlate with [F-18]-fluorodeoxyglucose uptake by positron emission tomography in epithelial tumors of the ovary. Int J Cancer 2004;109:926–932
21. Ito S, Nemoto T, Satoh S, Sekihara H, Seyama Y, Kubota S Human rhabdomyosarcoma cells retain insulin-regulated glucose transport activity through glucose transporter 1. Arch Biochem Biophys 2000;373:72–82
22. Guillou L, Coindre JM, Bonichon F, Nguyen BB, Terrier P, Collin F, et al. Comparative study of the National Cancer Institute and French Federation of Cancer Centers Sarcoma Group grading systems in a population of 410 adult patients with soft tissue sarcoma. J Clin Oncol 1997;15:350–362
23. Kawai A, Noguchi M, Beppu Y, Yokoyama R, Mukai K, Hirohashi S, et al. Nuclear immunoreaction of p53 protein in soft tissue sarcomas. A possible prognostic factor. Cancer 1994;73:2499–2505
24. Latres E, Drobnjak M, Pollack D, Oliva MR, Ramos M, Karpeh M, et al. Chromosome 17 abnormalities and TP53 mutations in adult soft tissue sarcomas. Am J Pathol 1994;145:345–355
25. Toffoli G, Doglioni C, Cernigoi C, Frustaci S, Perin T, Canal B, Boiocchi M p53 overexpression in human soft tissue sarcomas: relation to biological aggressiveness. Ann Oncol 1994;5: 167–172
26. Medina RA, Owen GI Glucose transporters: expression, regulation and cancer. Biol Res 2002;35:9–26
27. Strauss LG, Dimitrakopoulou-Strauss A, Koczan D, Bernd L, Haberkorm U, Ewerbeck V, et al. $^{18}$F-FDG kinetics and gene expression in giant cell tumors. J Nucl Med 2004;45: 1528–1535
28. Borbely K, Fulham MJ, Brooks RA, DiChiro G PET-fluorodeoxyglucose of cranial and spinal neuromas. J Nucl Med 1992;33:1931–1934
29. Beaulieu S, Rubin B, Djang D, Conrad E, Turcotte E, Eary JF Positron emission tomography of schwannomas: emphasizing its potential in preoperative planning. AJR Am J Roentogenol 2004;182:971–974

Eur Radiol (2006) 16: 1537–1543
DOI 10.1007/s00330-005-0091-3



**Ukihide Tateishi**
**Mototaka Miyake**
**Tetsuo Maeda**
**Yasuaki Arai**
**Kunihiko Seki**
**Tadashi Hasegawa**

# CT and MRI findings in KIT-weak or KIT-negative atypical gastrointestinal stromal tumors

Received: 25 July 2005
Revised: 28 September 2005
Accepted: 21 November 2005
Published online: 6 January 2006


U. Tateishi (✉) · M. Miyake · T. Maeda · Y. Arai
Division of Diagnostic Radiololgy and Nuclear Medicine,
National Cancer Center Hospital,
5-1-1, Tsukiji, Chuo-Ku,
104-0045, Tokyo, Japan
e-mail: utateish@ncc.go.jp
Tel.: +81-3-35422511
Fax: +81-3-35423815

K. Seki
Pathology Division,
National Cancer Center Hospital,
Tokyo, Japan

T. Hasegawa
Department of Clinical Pathology,
Sapporo Medical University
School of Medicine,
Sapporo, Japan

**Abstract** The large majority of gastrointestinal stromal tumors (GIST) can be diagnosed on the basis of KIT immunoreactivity. However, some atypical tumors show weak or negative KIT expression. We studied the imaging characteristics of atypical GIST, reviewing CT and MRI findings in ten patients (eight men, two women; mean age 59 years) with atypical GIST. Radiological studies were evaluated by two radiologists by consensus and included CT and MR imaging in all patients. Pathological diagnoses were made from surgery and confirmed by the polymerase-chain reaction (PCR) to amplify both exons of the c-kit gene and PDGFRA gene. The CT and MR examinations revealed a heterogeneous mass of the stomach containing cystic regions and soft tissue elements in all cases. All lesions were extraluminal masses and had an exophytic epicenter. On T1-weighted MR images soft tissue elements of the tumors were of homogeneously low- ($n$=3) or iso-signal intensity ($n$=7) compared with the liver parenchyma. On fast spin-echo T2-weighted MR images soft tissue elements of all tumors showed cystic regions of significantly high signal intensity interspersed with septumlike structures of low signal intensity. All lesions exhibited homogeneously ($n$=4) or heterogeneously ($n$=6) mild to moderate enhancement of soft tissue elements. Despite the relatively small number of patients CT and MRI findings of atypical GIST are a submucosal mass with soft tissue elements and cystic regions.

**Keywords** Gastrointestinal stromal tumor · Gastric tumor · Intestinal tumor · Stomach neoplasm

## Introduction

Gastrointestinal stromal tumor (GIST) is a mesenchymal tumor of the gastrointestinal tract that accounts for 2.2% of all gastric tumors [1]. According to a specific molecular analysis most GISTs express consistent immunoreactivity for KIT, a c-kit proto-oncogene protein (CD 117 antigen) [2]. The result of immunohistochemical survey leads to distinguish between GISTs and other mesenchymal tumors arising from the gastrointestinal tract [3]. Most GISTs have oncogenic KIT mutations that are early events in the pathogenesis of GISTs and result in the proliferation of tumor cells. Because of this a Kit-selective tyrosine kinase inhibitor, imatinib mesylate (Gleevec, formerly known as STI571; Novartis, East Hanover, N.J., USA) has been found to have a significant efficacy as a chemotherapeutic agent [4, 5].

Computed tomography (CT) and magnetic resonance imaging (MRI) have become a well accepted method for diagnosis and staging of GISTs [6–10]. The CT and MRI findings suggest that conventional GISTs are well-defined extraluminal or intramural masses, whose CT attenuation and MR signal intensity depend on tumor size. The larger tumors frequently appear heterogeneous as a result of central necrosis, cystic change, hemorrhage, and homogeneous tumors have a shorter diameter [6–10]. Nonspecific imaging features, however, have also been reported in various neoplasms, and one cannot rule out that a

mesenchymal neoplasm other than a GIST in gastrointestinal tract constitutes a potential drawback for successful imaging of GIST [11].

Although the large majority of GISTs can be diagnosed on the basis of KIT immunoreactivity, some neoplasms show weak or negative KIT expression [12–14]. They usually involve the stomach and are very rare, accounting for less than 5% of all GISTs and approx. 10% of gastric GISTs [15, 16]. As concerns such rare tumors, the weak or negative KIT mutation affects accurate pathological diagnosis for GIST. A recent cytogenetic study revealed the existence of mutations of the platelet-derived growth factor receptor α (PDGFRA) gene which was also the product of the c-kit proto-oncogene in KIT-weak or KIT-negative GISTs [17].

To our knowledge, no series focusing on KIT-weak or KIT-negative GISTs has yet been reported in the radiology literature. We therefore reviewed the imaging characteristics of ten atypical GISTs whose diagnosis was confirmed by pathological and cytogenetic analyses. We particularly focused on comparing the imaging characteristics that we observed with those previously reported.

## Materials and methods

A retrospective analysis of ten patients with KIT-weak or KIT-negative GISTs who underwent CT and MRI at our institution was performed (eight men, two women; mean age 59 years, range 43–73). Patients' medical database was reviewed for epidemiological, clinical and surgical findings. Nine patients presented with epigastric discomfort, nausea, vomiting or abdominal pain, and one mass was discovered when the patient was examined because of gastrointestinal bleeding at endoscopy. One had both abdominal pain and vomiting. All lesions arose in the stomach. Seven lesions were located in the body of the stomach, two in the antrum, and one in the cardia. Our institutional review board does not require its approval or patient informed consent for this type of review.

Radiological studies of each lesion were evaluated by two radiologists by consensus and included CT with and without contrast enhancement in all patients, and MR imaging with high-field (1.5-T) units in all patients. The CT examinations were performed with the patient in the supine position, and patients were also injected with iodinated nonionic contrast material (300 mg/ml iodine) intravenously at a rate of 3.0 ml/s for a total of 100 ml with an autoinjector. Patients were also given water of 300 ml as oral contrast. The scanning parameters of CT were: axial 4- or 16- slice mode, 1.0–5.0 mm section thickness, 0.5 s rotation, 120–150 kVp, 200–250 mA. Section thickness ranged between 5 and 10 mm by reconstruction using a standard algorithm.

T1- and T2-weighted MR images were obtained in the transverse plane and at least one longitudinal plane with a body coil. T1-weighted spin echo (SE) or fast spin-echo (FSE) acquisitions were obtained by using a 24–30 cm field of view, 4–8 mm section thickness, 400–620/8.9–15 (repetition time ms/echo time ms), 256×192–224 matrix, two signals acquired. T2-weighted FSE acquisitions were performed using a 24–35 cm field of view, 4–8 mm section thickness, 3,000–12,000/80–120 (repetition time ms/echo time ms), 256×192–224 matrix, and two signals were acquired. After the intravenous administration of 0.1 mmol gadopentate dimeglumine (Magnevist, Schering, Berlin, Germany) per kilogram body weight, transverse T1-weighted MR images with fat suppression were obtained in the transverse plane and at least one longitudinal plane.

Two board-certified radiologists retrospectively reviewed the CT and MR images, and their findings were reported as a consensus opinion. Images were evaluated for lesion location and size, shape of the interface (regular or irregular), endoluminal or extraluminal mass, epicenter (intrinsic or exophytic), cystic region, soft tissue elements, hemorrhage, intratumoral and capsular calcification, ulceration, central gas, fistula, infiltration of other organ, peritoneal dissemination, hepatic metastasis, enlargement of lymph node, ascites, and distant metastasis. MR images were evaluated for predominant signal intensity characteristics (low, intermediate, or high), signal homogeneity or heterogeneity, as well as enhancement characteristics. On T1-weighted MR images low signal intensity was defined as signal intensity less than that of muscle, intermediate signal intensity as similar to that of muscle, and high signal intensity as similar to that of fat. On FSE T2-weighted MR images low signal intensity was defined as signal intensity similar to that of muscle, intermediate signal intensity as greater than that of muscle, but less than that of fat, and high signal intensity as equal to or greater than that of fat. Tumor enhancement was visually graded as greater than, less than, or equal to that of surrounding muscle and vessels.

The cut surface, internal characteristics, and microscopic findings of the lesions were compared with the CT and MRI findings. Correlations between the imaging and histological findings were made by consensus between the radiologists and pathologists. Formalin-fixed and paraffin-embedded specimens were used for the histopathological and immunohistochemical studies and for the analyses for c-kit and PDGFRA gene mutations. A polyclonal antibody was used for KIT (DakoCytomation, Glostrup, Denmark, 1:50) [18]. Genomic DNA was extracted from formalin-fixed, paraffin-embedded specimens and amplified by the polymerase-chain reaction (PCR) to amplify exons 9, 11, 13, and 17 of the c-kit gene and exons 12 and 18 of the PDGFRA gene [15, 16]. We distinguished GISTs from leiomyosarcomas based on the immunoreactivity for KIT, desmin (DakoCytomation, 1:100), smooth-muscle actin (SMA; DakoCytomation, 1:100), and h-caldesmon (HCD; DakoCytomation, 1:100) [19].

Follow-up information was available in all cases. Follow-up contrast-enhanced CT examinations were per-

formed every 3–6 months after surgery. In one patient who was administered imatinib mesylate, follow-up contrast-enhanced CT was performed every month. Deaths confirmed to be caused by their disease were treated as an endpoint, and deaths from other causes were treated as censored observations. The disease-free date was recorded as the date when the medical record documented absence of any evidence of disease.

## Results

### Imaging findings

All lesions available for review on CT and MR examinations were detected (Table 1). Eight tumors had an irregular interface, and the other two had a regular interface. All lesions were extraluminal masses and had an exophytic epicenter. The average size of the tumors measured in the greatest dimension was 74 mm (range, 35–190 mm). The CT and MR examinations revealed a heterogeneous mass containing cystic regions and soft tissue elements in all cases (Figs. 1, 2, 3, 4). Unenhanced CT images of all lesions showed heterogeneous iso- ($n$=7) or hypo-attenuation ($n$=3) relative to the liver. None of the tumors had intratumoral or capsular calcification on unenhanced CT images. Soft tissue elements of the tumors were homogeneously ($n$=6) or heterogeneously ($n$=4) enhanced on contrast-enhanced CT images (Fig. 1). The attenuation of soft tissue elements was less than that of the aorta but greater than that of the liver parenchyma ($n$=7). Three tumors had soft tissue elements that were iso-attenuated relative to liver parenchyma on contrast-enhanced CT. In one tumor of the antrum the proportion of soft tissue element in the tumor predominated. Ulceration with detectable central gas was detected on CT in one lesion (Fig. 2). One patient had multifocal lesions and peritoneal dissemination (Fig. 3). Involvement of the gastrohepatic ligament was seen in three cases and involvement of the gastrosplenic ligament in two cases. On T1-weighted MR images soft tissue elements of the tumors were homogeneously low- ($n$=3) or iso-signal intensity ($n$=7) compared with the liver parenchyma. One lesion showed focal areas of high signal intensity, likely hemorrhagic regions. On FSE T2-weighted MR images soft tissue elements of all tumors showed predominantly increased T2 signal intensity relative to the liver parenchyma, and the images showed cystic regions of significantly high signal intensity interspersed with septumlike structures of low signal intensity (Figs. 2 and 4). All lesions exhibited homogeneously ($n$=4) or heterogeneously ($n$=6) mild to moderate enhancement of soft tissue elements and lack of obvious enhancement of cystic regions on contrast-enhanced MR images (Fig. 2). None of the CT or MRI images showed evidence of gastric fistula, liquefactive necrosis, infiltration of other organs, lymph node enlargement, or hepatic metastasis.

**Table 1** CT and MRI findings of atypical GIST

| | $n$ |
|---|---|
| Primary tumor | 10 |
| Interface | |
| Regular | 2 |
| Irregular | 8 |
| Extraluminal mass | 10 |
| Exophytic epicenter | 10 |
| Cystic region and soft tissue elements | 10 |
| Unenhanced CT attenuation | |
| Iso | 7 |
| Hypo | 3 |
| Enhancement pattern[a] | |
| Homogeneous | 6 |
| Heterogeneous | 4 |
| Enhancement degree* | |
| Hyper | 7 |
| Iso | 3 |
| MR signal intensity[a] | |
| T1-weighted image | Low 3, iso 7 |
| T2-weighted image | High 10 |
| Septumlike structure[b] | 10 |
| Secondary tumor | 3 |
| Peritoneal dissemination | 3 |
| Cystic region and soft tissue elements | 3 |

[a]Note. Imaging findings of soft tissue elements are presented
[b]Septumlike structure was depicted on T2-weighted image

### Pathological findings

The gross and microscopic characteristics of the resected specimens corresponded to the CT and MRI findings. All tumors were characterized macroscopically by soft tissue masses with cystic regions (Figs. 1 and 4). Myxoid degeneration was present in the cystic regions of seven lesions. One lesion had an irregular margin and exhibited central ulceration. Necrosis ($n$=3) and hemorrhage ($n$=1) were identified in the samples of four tumors. Histological examination revealed epithelioid cells presenting eosinophilic cytoplasm and peripherally placed nuclei with myxoid stroma in nine tumors (Fig. 1). In one case the tumor consisted of spindle and epithelioid cells in varying ratios. Three tumors were of high risk, two were of intermediate risk, and five were of low risk. Eight tumors showed weakly positive immunostaining for KIT and the other two tumors were completely negative. None of the tumors had a c-kit gene mutation. On the other hand, PDGFRA gene mutations were identified in all cases.

All patients but one underwent surgical resection as a primary therapy. The surgical margins were adequate in eight